Proceedings of the Twentieth (2010) International Offshore and Polar Engineering Conference
Beijing, China, June 20–25, 2010

ISBN 978-1-880653-77-7 (Set); ISSN 1098-6189 (Set); www.isope.org

Numerical Simulation of the Impact of a Plunging Breaker on a Vertical Structure and Subsequent Overtopping Event Using a Navier-Stokes VOF model

Cyril Mokrani
Laboratoire de Sciences Appliquées au Génie Civil et au Génie Côtier,
Anglet, France.
also at Centre Scientifique et Technique du Bâtiment, Université Paris-Est,
Marne-la-Vallée, France.

Stéphane Abadie
Laboratoire de Sciences Appliquées au Génie Civil et au Génie Côtier,
Université de Pau et des Pays de l'Adour,
Anglet, France.

Stéphan Grilli
Department of Ocean Engineering, University of Rhode Island,
Narragansett, Rhode Island, USA.

Kamel Zibouche
Centre Scientifique et Technique du Bâtiment, Université Paris-Est,
Marne-la-Vallée, France.

ABSTRACT

We study processes that occur during impact of a breaking wave on a vertical wall, and the resulting overtopping event, based on numerical simulations using a multiple-fluid Navier-Stokes VOF model (air-water). The latter allows to track high interface deformations during the breaking and impact. Both impact process and overtopping event are studied as a function of the relative distance of the vertical wall from the breaking point (defined as the location where a vertical tangent appears on the free surface). We study hydrodynamic forces and pressure peaks on the vertical wall, with the temporal and spatial discretizations. Expectedly, a finer discretization leads to a better description of the pressure peak on the wall, which can increase the total force applied to the wall by up to a factor 6. Similarly, we study, overtopping rates as a function of the distance of the breaking point in front of the wall. Some studies indicated that the critical case, yielding maximum volumetric rate, is for a wall placed at the breaking point. In the application studied here, the maximum overtopped volume of water occurs for a distance to breaking equal to 1.69 times the breaking wave height.

KEY WORDS: breaking waves, impact, maximum forces, peak pressure, overtopping.

INTRODUCTION

Improving the design of coastal defenses requires in-depth understanding of wave impact and overtopping phenomena. Various time scales are involved in these phenomena, which must be considered in work aimed at achieving such understanding. Many studies, more related to engineering applications, have focused on the larger time scales, by considering the cumulative effects of many waves, for instance on the total overtopping volume. However, individual wave and smaller time scales, must be considered in order to better understand the detailed flow that occurs during individual impact events. In this respect, the experiments of Schmidt et *al.* (1992) illustrated the effect of breaking point location has on the impact intensity on a vertical wall. Specifically, these identified four impact regimes, depending on the distance between the breaking point and the wall. Kirkgoz (1995) proposed a similar classification but identified three cases according to wave shape at the impact duration. In early numerical simulations, Grilli et al. (1992,1993) and Zhang *et al.* (1995) studied the impact of a two-dimensional plunging breaker on a vertical, wall using a Boundary Element Method (BEM). The former study showed the possible occurrence of very large impact pressures (and related vertical accelerations and total force). Zhang et al's work showed that the maximum impact pressures can be scaled by the local breaker parameters at impact. Although there were many other studies in the interim, based on inviscid flow theory, it is not our purpose here

to give an exhaustive review of the literature, and we just mention in closing the recent work by Duan *et al.* (2009), who studied the impact with a BEM of a plunging breaking wave on a vertical wall, by simulating an oblique collision of an asymmetric solid wedge. Pressure distribution near the wave tip were computed for many cases. BEM methods, however, cannot deal with post-breaking flows and cases of highly turbulent impacts. Models with more complete physics, such as based on the solution of Navier-Stokes (NS) equations, are required.

In this paper, we use Abadie et *al*'s (1998) et *al* and Lubin et *al.'s* (2006) NS-VOF model to investigate the impact force and overtopping flow generated by a large plunging breakers on a vertical wall. The effects of the distance between the breaking point and the wall, on the impact flow, are analyzed through numerical simulations. The paper is organized in five parts. We first briefly present the numerical model. The second part presents numerical experiments. Wave breaking stage is validated in the section 3 by comparing interfaces profiles computed by NS-VOF and BEM models during the breaking stage. The fourth and fives parts are devoted to the detailed analysis of wave impact forces and overtopping flows. Specifically, in the fourth section, we analyse breaking wave impacts obtained with two different meshes, and compare numerical results to experiments.. Section four brings into light differences induced by different meshes on the numerical simulation of the impact proper. Pressure time history and forces induced by impact are reported and analyzed in order to validate simulation of the impact process and determine the grid resolution required to model such impact process. Section five identifies the consequences of impact on fluids kinematics. Overtopping flow rates are reported and compared in different cases. Critical situations are highlighted and discussed in the final part.

THE MODEL

In our breaking wave simulations, we consider incompressible, non miscible two-phase flows of water and air, described by two-dimensional NS equations. As in Lubin *et al.* (2006), turbulence is resolved using a Large Eddy Simulation (LES) approach, with a Mixed Scale subgrid model. The interface between water and air is tracked using the Volume Of Fluid (VOF) method of Hirt and Nichols (1981). The water volume fraction evolution is calculated by solving a pure advection equation, assuming that the interface is moving at the fluid velocity.

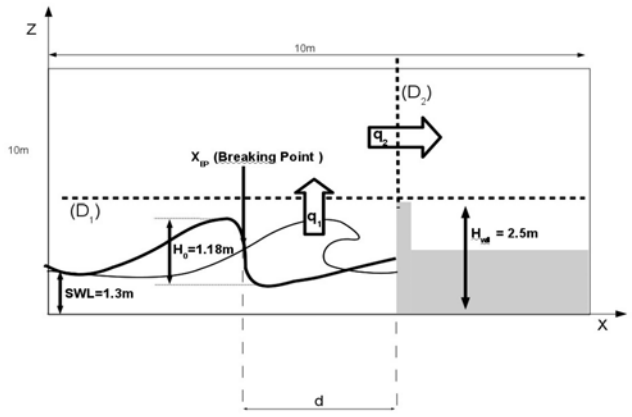

Figure 1: Sketch of physical problem

The NS-VOF equations are discretized on a fixed Cartesian grid, using a finite volume formulation. The coupling between velocity and pressure is solved using the augmented Lagrangian method (Fortin and Glowinski, 1982). The VOF equation is solved using a TVD superbee scheme (Vincent and Caltagirone, 1999). The latter is a Lax Wendroff scheme, modified by using the Total Variation Diminishing theory (Le Veque, 1990), which allows to preserve sharp discontinuities through time updating, without triggering oscillations (such as observed with higher-order schemes).

The resulting linear algebraic system of equations, obtained for each time step, is solved using the direct solver MUMPS (Multifrontal Massively Parallel sparse direct Solver (Amestoy *et al.*, 2000)). At the end of each time step, the average water volume fraction in each cell is used to recalculate local values of density and viscosity used in NS equations. For cells containing a fraction of water and air, equivalent density and viscosity are calculated by linearly interpolation based on the water fraction *F*.

DESCRIPTION OF NUMERICAL EXPERIMENTS

The physical problem considered is sketched in Fig.1. All computations have been done in a square domain, 10 meter high and 10 meter long, with an initial constant depth of 1.3 meter. As we concentrate here on modeling the impact processes, we simply initialize computations with a first-order Stokes wave of non-physical height, which rapidly evolves to breaking, as a large scale plunging breaker, close to the wall. Parameter *d* represents the distance of the wall to the breaking point, which is made to vary by adjusting the position of the wall, given a breaking wave. The breaking point is defined as the location where the inflection point of the free surface profile has a vertical tangent. All computations have been performed using the same wave characteristics, detailed latter. Two different model grids (coarse and finer) were tested, in order to assess the required mesh size to correctly model impact and interface deformations. Mesh sizes are identical in horizontal and vertical directions. The coarser mesh has spatial steps of 0.05 m while the finer mesh has steps of 0.0125 m. The total corresponding number of nodes in the discretization are 40,401 and 641,601 respectively. Time step is computed by specifying a mesh Courant number less than 0.3 .

Computations of impact have been done in two stages. A first-order Stokes wave is generated and propagates in the domain, assuming periodic boundary conditions at the left and right domain sides.

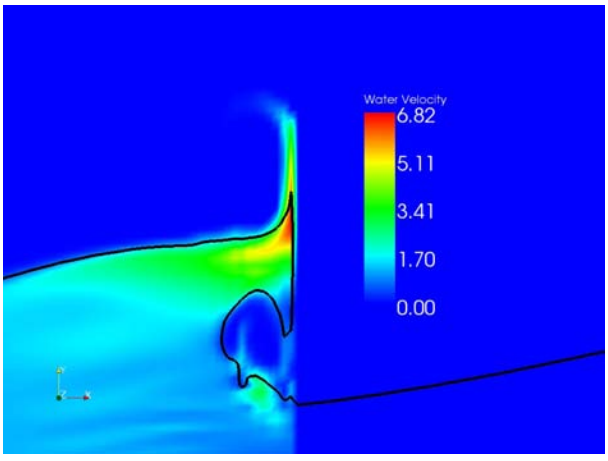

Figure 2: NS-VOF simulations of breaking wave impact on a vertical wall

An open boundary condition is imposed at the domain top to allow air

to escape without influencing water flows. At the bottom, a free-slip condition is imposed. The initial wave period is T_0 = 3.024 s and the wave height is specified equal to the still water level: $a_0 = SWL$ = 1.3 m. Parameters l_0 and H_0 represents respectively the wavelength (l_0 = 10m) and the wave height at the breaking point. The large value of wave steepness (ε = 0.13) leads the computed wave to rapidly become unstable and develop a large plunging breaker jet. Those characteristics correspond to the case studied by Vinje et al.(1981) using a BEM. A comparison of free surface profiles and kinematics, between NS-VOF and BEM model results, is provided in Section 3.

After the breaking point is reached, computed waves characteristics and shapes are recorded and used to directly initialize impact computations on a vertical wall. Impact computations are performed in a domain of similar dimensions. Boundary conditions on the left and right sides are changed from periodic to symmetrical. The vertical wall is placed on the right side (Fig. 1). It is designed as a crown wall, followed by a reservoir in which overtopping water will collect. This will allow assessing overtopping rates occurring during the impact process. In successive numerical experiments, the wall distance ahead of the breaking point is varied from d = 0 to 3 m, with a constant space step Δd = 0.25 m. In the following we refere to non-dimensional distance $d^* = d/H_0$ (d^* = 0 to 2.536 with $\Delta d^* \sim 0.21$). In addition, all non-dimensional parameters are noted with the exponent *. The wall height is H_w = 2.5 m for all computations, which proved low enough to yield significant over topping events.

In the multiple-fluid numerical model, the structure to the right is simulated as a porous media with infinite porosity, using a penalty method. This imposes a velocity equal to zero on the obstacle (no flow), and forces fluids particles to abruptly change direction (essentially from horizontal to vertical) when collision occurs. Fig. 2 shows the effect of such a porous media on both velocity magnitude in water and interface (black line). Such change in velocity direction are quantified by measuring the flow rates across vertical and horizontal lines. In Fig. 1, D_1 is horizontal level placed at height H_{wall}, while D_2 is a vertical line localized at the wall abscissa. In all cases, flow rates q_1 and q_2 are calculated during the impact process for further analysis.

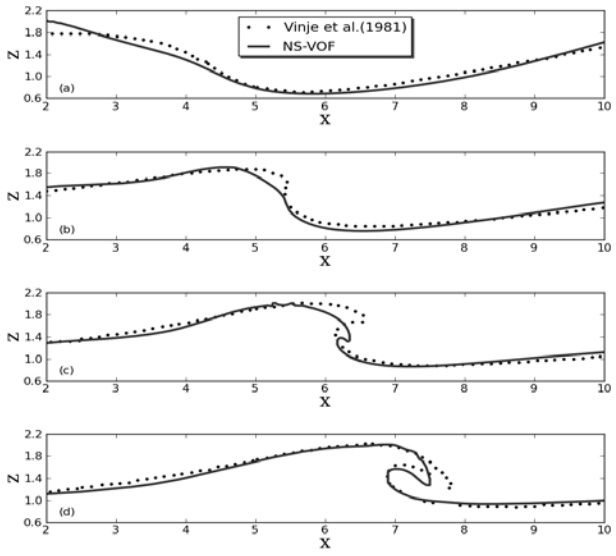

Figure 3: Plunging breakers simulated in NS-VOF and BEM models. (a) t = 0.17T_0 (b) t = 0.3T_0 (c) t = 0.38T_0 (d) t = 0.46T_0

BREAKING STAGES

Figure 3 shows the initial instability and evolution to breaking stages of a first-order Stokes waves of initial characteristics l_0 and T_0 mentioned before, computed with both 2D-NS-VOF and 2D-BEM models. This configuration corresponds to a large wave propagating in shallow water. Given the high value of steepness (ε=0.13) and relative height, the first-order Stokes theory is no longer valid and the initial wave is highly unstable, as illustrated in Fig. 3, and rapidly evolves towards a large plunging breaker. In Fig. 3, the NS-VOF solution obtained at different times is compared with Vinje et al.'s (1981) BEM solution. Differences between results are discussed in the following. The wave height at the breaking point is assessed to H_0 = 1.18 m with NS-VOF model. Computations yields a breaking point located at X_b = 5.7 m, which occurs at t = 0.997 s, whereas in the BEM solution the breaking stage starts after 0.925 s, when the wave crest is located at X_b = 5.3 m. Such small differences may be due to numerical diffusion induced by the VOF-TVD method used to track interface deformations, well-known in such numerical algorithms. The energy, which is numerically dissipated during the wave propagation stage, may also lead to a reduced wave celerity and thus a delay in reaching the breaking point and the following hydrodynamics processes. However, interface profiles, especially the rear of the wave crest, agree reasonably well for the three last times. The asymmetry of the wave profile is more pronounced in the BEM model at $t = 0.3T_0$ since breaking is already initialized, despite the NS-VOF showing a deeper trough. At $t = 0.38T_0$, the plunging jet is more developed in the BEM model and is at a higher position (likely due to the lack of energy dissipation in the BEM model). The plunging jet is downward in the BEM case and seems to contain more fluid particles. Even if jet direction and dimension are not similar at this time, kinematics of fluids particles present in the wave crest seem similar enough and to have the same behavior. Plunging jet characteristics become more and more similar with increasing time. The overturning part of the wave and the final ejecting jet have more similar shape and orientation at $t = 0.46T_0$.

In order to improve the breaking wave shapes simulated in the NS-VOF model, a coupling approach using actual BEM solutions, similar to Guignard et al. (1999), is in progress. This will also lead to refining interface tracking during the breaking stage until the impact time. However, in the following sections, impact is computed based on wave characteristics shown in Fig.3, with parameter d^* ranging with constant space step (d = 0 to 3 m).

IMPACT PROCESSES

As we will demonstrate, it is difficult to precisely know the actual impact forces applied to vertical walls in our specific configuration and modeling approach. However, various studies available in the literature give guidance as to the expected orders of magnitude. For instance, Zhang et al. (1996) performed comparisons between experimental results and numerical computations of breaking wave impacts on a vertical wall. Plunging impacts were computed for wave amplitudes ranging from 0.1 to 1 m, in one meter water depth. They showed that maximum pressure was reached at about 0.16 m above the still water level. Moreover, computed values of maximum pressure were about 198 kPa. They were reached nearly 0.003 seconds after the initial stage of impact (this data will be pointed as rising time and noted t_{rise} in the following). However, maximum pressures recorded during quasi similar experimental tests only reached 58.8 kPa. Other experimental tests performed by Schmidt et al. (1992) constitutes another good means of validation of our simulations, as they measured impact forces of large plunging breakers generated by periodic waves. In their cases, maximum impact forces reached 316 kN/m and maximum pressures

300 kPa, for 1.5 meter high tested waves. The Fig. 4, reproduced from Schmidt et al. (1992), shows the time evolution of the applied horizontal force on a vertical wall during the impact process, in two time scales. The first one at larger time scale (little frame at the right) shows one pronounced peak force, reaching about 200 kN/m, then a second moderate increase in force, with a longer duration and a local maximum of about 50 kN/m. This second maximum value in the force is reported to be reached at the run-up time, that is to say, when the water interface reaches its maximum height on the wall during impact. The main frame in Fig. 4, at finer time scale, allows to see that in fact the first peak consists in two separate peaks, of which the first is smaller than the second one. Experimental measurements identified the expected impact force duration, defined here as the duration between those two successives force peaks, at about 20 ms. Moreover, falling time assessed from the second peak is about 30 ms. Those peaks are followed by relatively lower frequency oscillations which are reported to be caused by expansions and compression of the air pocket entrapped between the plunging breaker and the wall, under the highly transient pressure field. Since our numerical model does not take compressibility into account, this phenomena will not be discussed here.

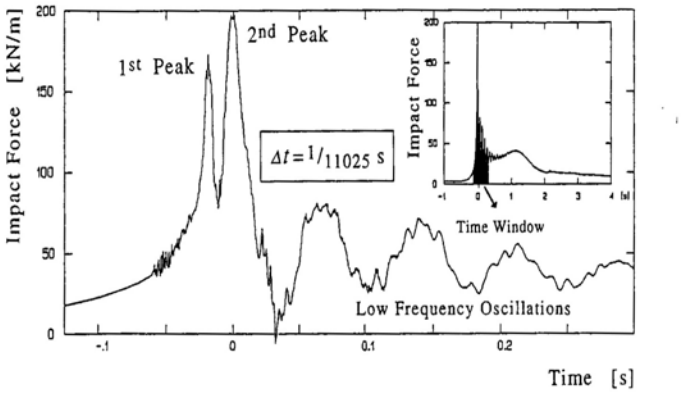

Figure 4: Force history - Shmidt et al. (1992)

In the following, we model the impact process for the same incident breaking wave (discussed before), for 13 different d^* values ranging from 0 to 2.53 (which is equivalent to d ranging from 0 to 3 m) with a constant step $\Delta d^* \sim 0.21$ ($\Delta d = 0.25$ m). For clarity, only cases d* = 0, 0.422, 0.845, 1.268, 1.690, 2.113, and 2.536 are discussed in the following.

Figure 5 shows the time evolution of the simulated horizontal impact force applied to the wall (Fig.1), using a coarse grid, for various cases of d^* parameter. In these simulations, horizontal and vertical non-dimensional space steps are $\Delta z / H_0 = \Delta x / H_0 = 0.0422$ ($\Delta x = 0.05$ m). The total node number is 40,401. The total force applied on the vertical wall is calculated by integrating the fluid pressure on the obstacle. Non-dimensional results are shown, based on a characteristic force : $F_0 = P_0 H_0 = \rho_0 c_0^2 H_0$ with $\rho_0 = 1000$ kg/m^3, c_0 and P_0, representing respectively the characteristic pressure, and the mean particles velocity calculated on the vertical line locates at the breaking point. The latter has been assessed to $c_0 = 3.30$ m/s, also equal to the linear wave celerity given by l_0/T_0 (with T_0 the wave period). Time values have been made non-dimensional by using $t_0 = h_0 / c_0 = 0.35$ s. During computations, time steps range around 10^{-3}s. As the impact duration is expected to be about 10^{-1} to 10^{-3} s (Zhang et al., 1996), we also expect this parameter low enough to correctly describe the impact processes.

Globally, forces histories in Fig.5 have identical behaviors, that is, a rapidly increasing force until a maximum value, and then a more gradual decrease and stabilization around a constant value (≈ 1.5). Critical cases are identified for $d^* = 1.268$ ($d = 1.5$ m), for which the maximum values reach 3.75, that is almost 50 kN/m. The width of the force peak seems to decrease, the larger d^*, until the critical case is attained, and then to become wider until the last value of d^*.

Figure 6 details the force time history for the particular case of $d^* = 1.268$. In this figure, axes are dimensional values of forces and time, in order to facilitate the comparison with Schmidt and al.'s (1992) results. Comparing numerical results in Fig. 6 with experimental measurements in Fig. 4, we see that the maximum computed force in the coarse grid is significantly smaller, with 200 kN/m (=15.47 in our non-dimensional conventions) for Schmidt and al. (1992) experimental results versus 50 kN/m for NS-VOF simulations (= 3.7 in our non-dimensional conventions). In addition, falling time is assessed to 0.5 s, which is much low than in Schmidt and *al.*'s study (30 ms). However, it should be stressed that experimental results are subject to wide scatter, as pointed out, e.g., by Kirkgoz (1982) where experimental impact loads varied drastically for apparently identical wave impacts. In fact, the high sensitivity of impact forces on a vertical wall to small variation in incident wave in both experiments and simulations, has already been identified in many works (e.g., Grilli et al., 1993). Further to this, in Zhang et al.'s (1996) experimental results, initial wave amplitudes were higher than ours and maximum forces only reached about 30 kN/m, in experimental conditions closer to ours.

As the total force applied to the wall is obtained by spatially integrating the pressure distribution, if the latter is underestimated then dynamic pressure applied to the wall must be too small on the wall. Hence, in order to better validate our simulations of impact processes, we have to study the sensitivity of maximum pressure on the wall to numerical and other parameters and establish sufficient result convergence.

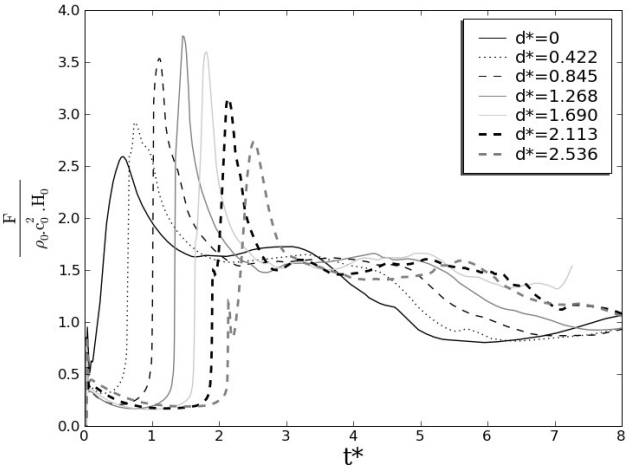

Figure 5: Time evolution of impact force in NS-VOF simulations - Coarser mesh grid

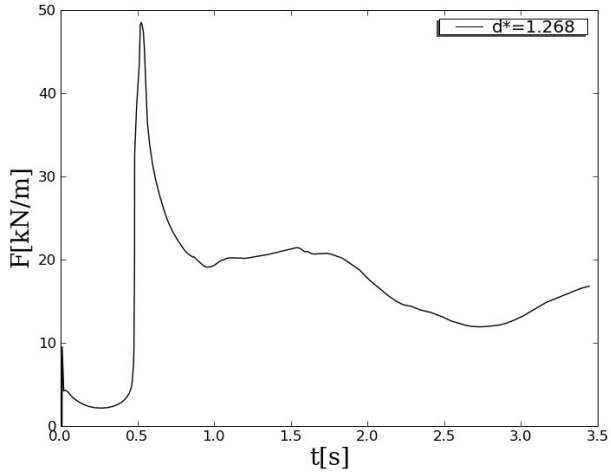

Figure 6: Force history - Case $d^* = 1.27$ - Coarse mesh grid (same as curve in Fig. 5 using dimensional parameters)

Figure 7 shows the time evolution of the maximum pressure reached on the wall during the impact process, for various values of parameter d^*, similar to Fig.5. We see these pressure variations are qualitatively similar to those in Fig.5, with the difference that critical maximum pressure is reached for the case $d^* = 1.69$. Maximum impact pressure is 3.66 (= 40 kPa), which is of the same order of magnitude as measured in Zhang et al. (1996) (P_{max} = 58.8 kPa, P^*_{max} = 5.38), but far less than results of Schmidt et al. (1992) (P_{max} = 300 kPa, P^*_{max} = 27.45). It is noted that impact pressures have faster variations in time the larger d^*, except for d* = 2.536 (d = 3m). However, observed rising times range from 70 ms (d* = 0) to 170 ms (d* = 1.69), which is much more than in Zhang et al.'s (1996) results (t_{rise} = 3 ms). Thus, the simulated evolution of impact pressure seems not fast enough in the case of the coarse grid.

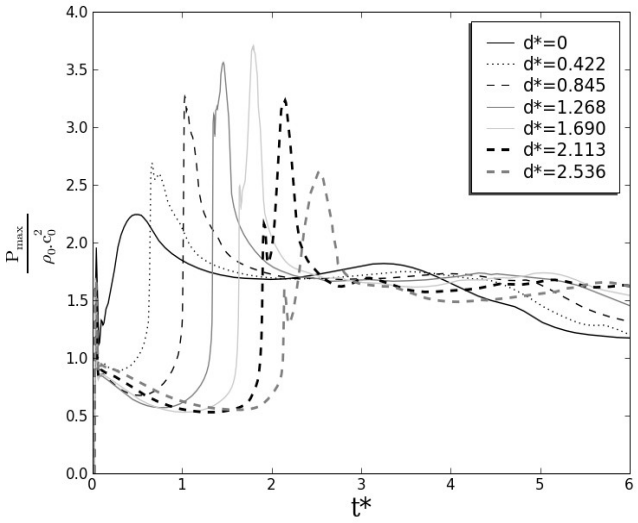

Figure 7: Maximum pressure history - Coarse mesh grid (same cases as in Fig. 5)

To improve on this, we model the impact process in a finer numerical grid, in order to better track the pressure peak. The second finer mesh used here contains 15 times more grid points than the coarse one. Non-dimensional space steps are divided by a factor of 4 ($\Delta x/H_0$ = 0.0105), and the CFL condition constrains the time step to be around $\approx 10^{-4}$ s. The total node number is then 16 times more important. Figure 8 shows the force time history for the same range of d^* parameters, in the case of a fine mesh. Note, as compared to Fig. 5, that the initial instants of impact are not the same, because the initializations of computations have not been made at the same instant. Thus, impact times are slightly delayed as compared to previous figures. However, since important characteristics are the impact duration and the maximum forces involved during the impact process, this delay does not influence the following analyses.

In Fig. 8, we observe different force evolutions, as compared to the previous coarser grid case. Maximum forces values range from 3.79 for $d^* = 0$ to 20.9 for $d^* = 1.69$, that is F_{max} = 273 kN/m. Note that this value is almost 6 times larger than the maximum value found in the coarse grid. Time variations of forces near the peak are wider than for the first tested cases ($d^* = 0$, 0.422 and 0.845) but rapidly become narrower, the higher d^*.

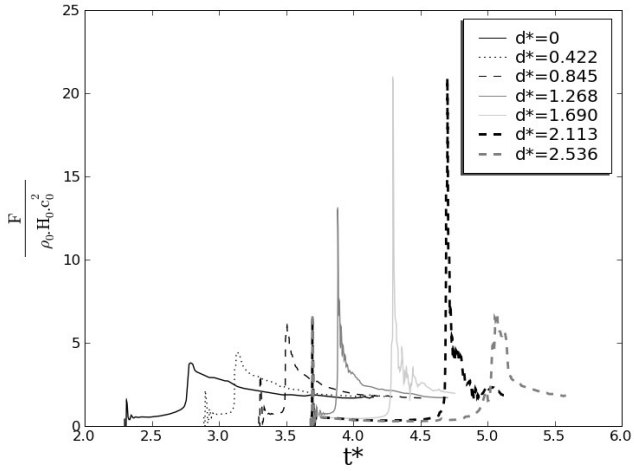

Figure 8: Force history for cases similar to Fig. 5- Fine mesh grid computations

Hence, falling times (defined as the duration between the initial stage of impact and the instant when the first peak is reached) are larger for smaller values of d^*. The impact force rate of increase prior to the peak is also larger in Fig. 8, as compared to the previous case. Rising times involved are smaller than those computed in the coarse grid case. In these finer grid simulations, maximum forces agree better with Schmidt al's (1992) or Plumerault's (2009) experimental results, as they both found that the total force for a periodic wave impacting a vertical wall could reach more than 100 kN/m, for similar wave characteristics. Note also that the case $d^* = 1.268$, which corresponded to the critical force for the coarse mesh no longer yields maximum impact force values but rather it now occurs for $d^* = 1.69$.

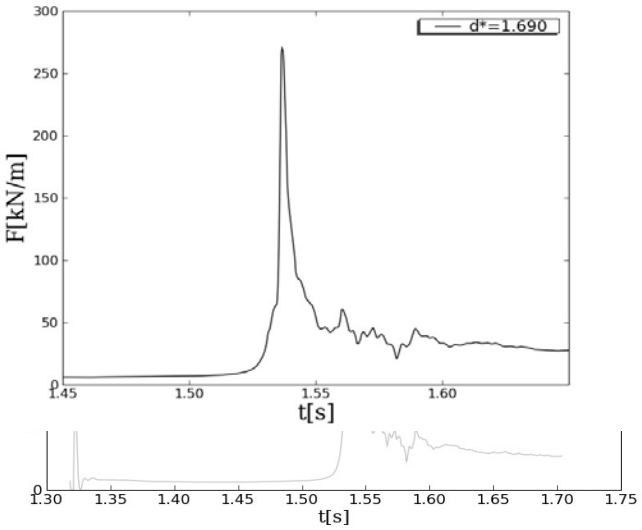

Figure 9: Force history - fine mesh grid – Case d*=1.69

Figures 9 details the force time history for the particular case of d^* = 1.69. Other computations, using even finer mesh grids are ongoing (which should be presented during the conference), to study the convergence of pressure peak in similar cases. For the represented case, both maximum computed force (273 kN/m) and force falling time (15.7 ms) are closer to Schmidt et *al*. (1992) (316 kN/m, 30 ms). Figure 10 shows non-dimensional pressure variations corresponding to the cases in Fig. 8. In this case, critical case is observed for d^*=2.113. In Figure 10, we can observe that rising time are lower than in the coarser grid. Figure 11 represents the iso-line of pressure peaks. This illustrates how fast the wall pressure may vary since maximum pressure peaks are reached in less than 0.004 s. This agrees well with Zhang et *al.'s* (1996) results (0.003 s).

It was shown above that time steps used in coarse grid simulations were too large to accurately capture the pressure peaks during impact and the resulting force variations applied to the wall. Impact process proved to be better describe for refined mesh grid and time step ranging around 10^{-4}s. The convergence of results must be proved on finer mesh grid, but finer discretization leads to a better description of the pressure peak on the wall.

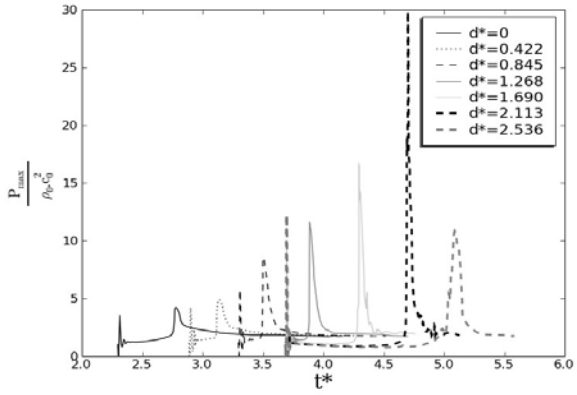

Figure 10: Maximum pressure - Fine mesh grid

OVERTOPPING FLOW RATE

We now investigate overtopping rates, which are direct consequences of the impact process. Overtopping event have been investigated experimentally and numerically, but with very limited success. Experimental difficulties to obtain significants values are often due to large parameters involved in such a process (wave shape, wall roughness, porosity, geometric wall shape, wall position, wind magnitudes, salted rate in water, presence of air entrapped, entrained ...), or to difficulties in establishing permanent regime during green water events. Such a problem is also hard to tackle with numerical models, as this involves complex simulations of fast moving, multiphase, and highly turbulent flows after a collision with a vertical wall. Few experimental studies successfully measured velocity of breaking waves impinging on structures.

Among, those, several applied the dam break theory to green water modeling, as mentioned in Buchner (1995a,b), even though the similarity between dam break and green water has not been quantitatively verified. Ryu et al. (2007) performed an experimental study, based on a PIV method, to measure the kinematics of plunging breaking waves impinging on and overtopping a model structure with a deck. Breaking waves were generated in front of a model, using a frequency focusing method, and conditions were fixed to be as close as possible to maximum waves that can occur during severe storm events. For such conditions, wave period, wavelength, wave height near the structure, phase speed of the breaking wave, and water depth were respectively 1.29 s, 2.54 m, 0.17 m, 1.95 m/s, and 0.80 m at model scale. The tested structure contained no tank, in order to analyze velocity profiles on the deck. In such conditions, wave heights were more important than wall height (equal to 91 cm), which was almost 3 times H_{wall} (defined in section 2, H_{wall} = 2.5 m). Based on Froude scaling, the equivalent full scale wave had a height of 28 meters. Thus, the represented impact corresponds to a far more critical case of impact and resulting over topping event than in our configuration. However, Ryu et al.'s study provided interesting result regarding velocity profiles near the structure and flow behavior after impact. For instance, before the wave impinged on the structure, the maximum water velocity near the structure reached 1.5 times the wave celerity. After impact, the flow tended to follow the boundary of the obstacle, with dominant vertical velocities reaching 2.9 times the wave celerity. In the following, we compare our velocity magnitudes with those values.

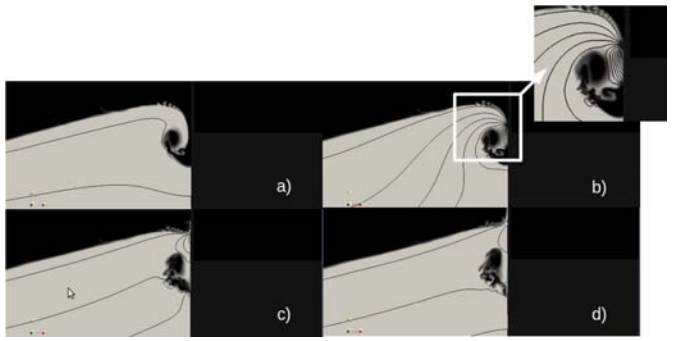

Figure 11: Iso-line of pressure peak - Fine mesh at
a) t* = 0.485, b) t* =0.495 , c) t*=0.498 , d)t*=0.504

Fig. 12 shows three snapshots of free surface elevation and velocity magnitude at the time of maximum upward jet motion, for d^* = 0, 0.845, and 1.69. In the first case, at t^* = 2.71, the air pocket is negligible, as the wave just begins to break when it impacts the wall.

Velocity is maximum at the tip of the jet. The computed value is about 3.3 times the breaking wave celerity. The second case is for *d*=0.84* at *t*=3.23*. Here, we see a more developed air pocket. This instant corresponds to the generation of the upward ejected jet. Maximum velocity reaches about 3.77 times the wave celerity. In the third snapshot, for *d*=1.69,* at *t*=3.84*, the wave breaking is well advanced and the impact occurs at the apex of the breaking jet. In this case, there is a large size air pocket captured, since the reconnection between the breaking jet and the free surface has occurred. Maximum velocity reaches about 6.75 times the wave celerity at the top contact point between jet and wall. Note that this value is larger than in Ryu et al.'s (2007) experiments, and than the order of magnitude of the two previous cases. Since the wave is lower than the wall, and the numerical wall cannot absorb any mechanical force, a large part of the kinetic energy of the fluid can be devoted to the generation of an upward jet. This justifies why upward velocities in this case should be important, leading to larger values of over topping flow rates.

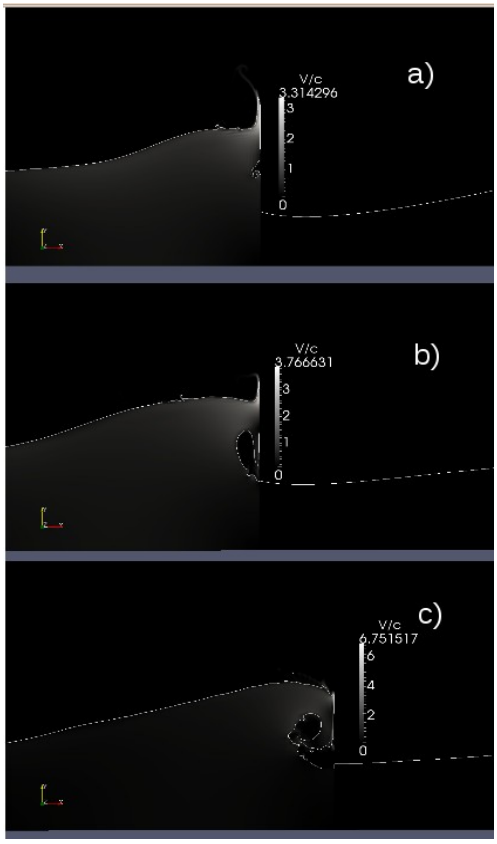

Figure 12: Velocity magnitude at the time of maximum upward jet velocity.
a) d*=0, t*= 2.71 , Vmax/c_0=3.31, b) d=0.84, t*=3.23 Vmax/c_0=3.77, c) d*=1.69, t*=3.84 , Vmax/c_0=6.75

Volumetric flow rates across D_1 and D_2 have been calculated from impact computations on a coarse mesh grid, and reported on Figs. 13 and 14. Flow rates have been made non-dimensional by $Q_0 = (g H_0^3)^{0.5}$, representing the characteristic rate across a vertical line whose elevation is H_0.

Figure 13 shows time series of volumetric flow rates across the horizontal line D_1, for different values of parameter *d**. Flow rate evolutions have globally similar behaviors. Flow rate values increase until a maximum value is reached, then decrease until they reach negative values. These correspond to the beginning of the jet down-rush. In all cases, flow rate variations are rapid near the maxima. Then, flow rates oscillate around zero. We also observe a second local minimum of flow rate, which corresponds to the reflected wave off the wall. This second local minimum occurs in all cases but it is the most pronounced for *d** = 0, for which the nearly non-breaking wave mostly reflects off the wall. Maximum values of horizontal flow rates increase with *d** except for the last case *d** = 2.53 (d=3m), for which the maximum value is similar to the case *d** = 0. The critical case (for which flow rate is maximum) is for *d** = 2.11 (d=2.5 m). In this configuration, maximum flow rate is about 0.25, that is ~ 1 m^3/(m.s).

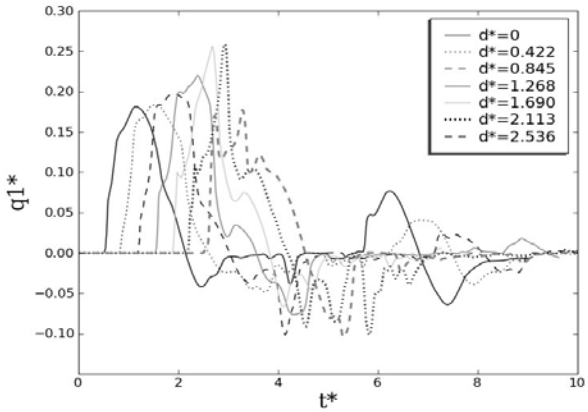

Figure 13: Volumetric flow rate across D_1 (Fig. 1)

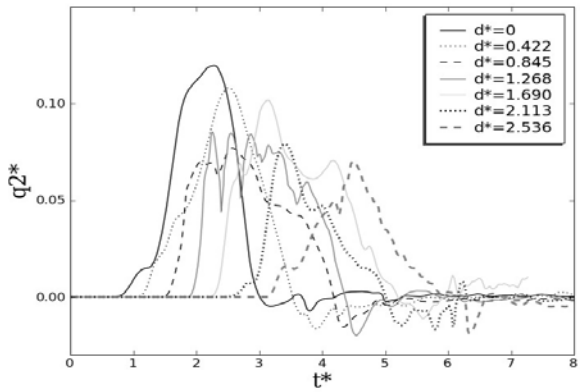

Figure 14: Volumetric flow rate across D_2 (Fig. 1)

The total volume corresponding to the vertical and horizontal flow rates was calculated by integrating the flow rate in time until the time it becomes negative. The fact that flow rate increases up to *d**=1.69 (*d*=2 m) is in good agreement with analyses based on velocity magnitudes presented above.

The same experiment was performed on the vertical line D_2 placed between the top of the tank and the top of the domain (Fig. 1). Results of flow rates across D_2 are represented in the Fig. 14, as a function of *d**, to assess the final amount of water in the tank. Flow rates have similar overall behaviors, that is, an increasing flow rate until a maximum is reached, followed by a decrease to zero. Negatives values correspond to the presence of negative horizontal velocities, of particle sinking along the wall when the downward phase is over. These however are negligible for all cases tested, compared to flow values computed during the whole overtopping event. Flow rate evolutions become slower with increasing *d**. Actually, flow rates across D_2 are seen to vary as rapidly as overtopping flow rates (see previous

paragraph). A second local maximum value appears for the case d^* = 1.69. The case d*=1.268 has various maximum values and a more specific behaviour. This is due to the presence of a secondary jet at the

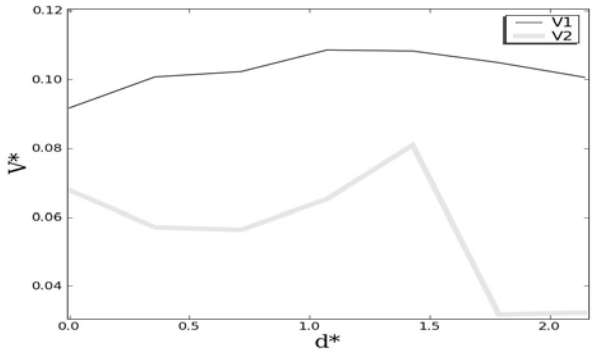

Figure 15: Total overtopped water volume for various values of d^*

moment of impact which ejects water particles behind the wall. However, we did not take this case into account before validate it on a finer mesh grid. The overall maximum value is obtained for the first case $d^* = 0$, with a flow rate of about 0.11that is 0.43 $m^3/(m.s)$. The accumulated volumes for flow rates across D_1 and D_2 are given in Figure 15 as a function of the distance d^* of the vertical wall to the breaking point. Values of volume have been made non-dimensional using $V_0 = (H_0)^3$. The figure shows that the total volume accumulated across D_1 ($=V_1$) has one maximum. This maximum (V* = 0.11) appears for the critical point, for which d^* = 1.69 (d=2m). Maximal volume is reached for this value as well, and two local minimum values occur for extreme values of d^*.

CONCLUSIONS - DISCUSSION

A NS-VOF model was used to investigate the impact force on a vertical wall, and the related overtopping rate, generated by a large plunging breaker. First, the wave breaking stage was validated by modeling the time evolution of a first-order breaking Stokes wave and comparing interface profiles with earlier BEM model results. A coupling approach, between a BEM solution and the NS-VOF model is in progress, to refine interface tracking during the breaking stage, until the time of impact, and it is expected that initial results will be presented at the conference.

The impact processes modelisation has been considerably improved by refining mesh grids. The comparison between numerical results and existing laboratory experiments and other studies present in literature have been used as references in numerical solutions. We showed that computations using a fine resolution mesh have good accuracy to describe the time history of the impact forces on the wall as described in Schmidt et al. (1992) and Zhang et al. (1996), particularly around its short duration peak. Using two different meshes grid showed that multiplying the total number of grid cells by a factor of 15 leads to a better description of the pressure peak on the wall, and to a total force applied on the wall larger by a factor of 6. Convergence of maximum pressure and force applied on the wall is still to be proved.

Overtopping events generated after the impact were studied. The magnitude of flow velocities was computed and compared with Ryu et al.'s (2007) experiments. The larger overtopping rates and flow velocities occur for a particular distance of the wall to breaking, which in the present case corresponds to d^* = 1.69 (d=2m). The influence of the parameter d* on overtopping flow rates was specifically studied. Velocity magnitudes near the wall reached extreme values for d*=1.69. The resulting flow rates were maximum for the same case.

REFERENCES

Abadie S. , Caltagirone J. P. & Watremez P., 1998, "Splash-up generation in a plunging breaker" . Comptes Rendus de l'Académie des Sciences - Series IIB – Mechanics-Physics Astronomy, Volume 326, Issue9,Pages 553-559.

Amestoy PR, Duff IS and L'Excellent J. (2000). "Multifrontal parallel distributed symmetric and unsymmetric solvers." *Comput. Methods in Appl. Mech. Eng.* **184**: 501-520.

Buchner B (1995a). "The impact of green water on FPSO design". Offshore technology Conference, Houston, OTC 7698:45-57.

Buchner B (1995b). "On the impact of green water loading on ship and offshore unit design." In P*roc. 6th International symposium on pratical design if ships and mobile units* (PRADS), pps. 1403-1443. .

Duan, W.Y., Xu, G.D. Xu, G.X. (2009). "Similarity solution of oblique impact of wedge-shaped water column on wedged coastal structures ". *Coastal Engineering* **56** : 400–407.

Fortin M, Glowinski R. (1982). "Méthodes du lagrangien augmenté. Application à la résolution numérique de problèmes aux limites." Dunod, Paris.

Grilli, S.T., Losada, M.A., Martin, F. and Svendsen, I.A. (1992). "Nonlinear Shoaling and Impact of Waves on Coastal Structures." In *Proc. 9th Engineering Mechanics Conf.* (College Station, Texas, May 92) (eds. L.D. Lutes and J.M. Niedzwecki), pp. 79-82. ASCE edition.

Grilli, S.T., Losada, M.A. and Martin, F. (1993). "Wave Impact Forces on Mixed Breakwaters." In *Proc. 23rd Intl. Conf. on Coastal Engineering* (ICCE23, Venice, Italy, October 92) Vol. **1**, pps. 1161-1174. ASCE edition.

Guignard, S., Grilli, S.T., Marcer, R. and Rey, V. (1999). "Computation of shoaling and breaking waves in nearshore areas by the coupling of BEM and VOF methods." In *Proc. 9th Offshore and Polar Engng. Conf.* (ISOPE99, Brest, France, May 1999), Vol. **III**, 304-309.

Kirkgoz M.S. (1982). "Shock pressure of breaking waves on vertical walls". *J. Waterways, Port Ocean Engng.,* **108**:81-95.

Kirkgoz M.S. (1995). "Breaking wave impact on vertical and sloping walls". *Ocean Engineerin*g **22**(1):35-48.

LeVeque RJ. (1990). *Numerical Methods for Conservation Laws.* Lectures in Mathematics. Birkhauser, Zurich.

Lubin P, Vincent S, Abadie S, Caltagirone JP. (2006). "Three-dimensional Large Eddy Simulation of air entrainment under plunging breaking waves". *Coastal Engineering*, **53**(8): 631-655.

Plumerault L.R. (2009). "Numerical modelling of aerated-water wave impacts on a coastal structure." 136p.

Ryu Y. , Chang K-A, Mercier R. (2007). "Runup and green water velocities due to breaking wave impinging and overtopping". *Exp. Fluids,* **43**:555-567.

Schmidt R., Oumeraci, H. and Patenskyn H. W. (1992). "Impact loads induced by plunging breakers on vertical structrures." In *Proc. 23rd Intl. Conf. on Coastal Engineering* (ICCE23, Venice, Italy, October 92) Vol. **1**, pps. 1545-1558. ASCE edition.

Vincent S, Caltagirone JP. 1999. Efficient solving method for unsteady incompressible flow problem. *Int. J. Numer. Methods Fluids,* **30:** 795-811.

Vinje T. , Brevig P. (1981). "Numerical simulation of breaking waves", *J. adv. Water Resour*. **4:**77-82.

Zhang S., Yue D.K.P., Tanizawa K. (1996). "Simulation of plunging wave impact on a vertical wall". *J. Fluid. Mech*., **327:**221-254.